Influence of Interphase on Tensile Behavior of Strain Hardened AA1100/AlN Nanocomposites Using RVE Models and Experimental Validation

A. CHENNAKESAVA REDDY

Professor, Department of Mechanical Engineering, JNTUH College of Engineering,
Kukatpally, Hyderabad 500 085, Telangana State, India.
acreddy@jntuh.ac.in

Abstract

In this article three schemes of RVE models, namely without interphase, with interphase and with voids and interphase, have been implemented using finite element analysis. Aluminum nitride (AlN) nanoparticles were used as a reinforcing material in the matrix of AA1100 aluminum alloy. It has been observed that the nanoparticle did not overload during the transfer of load from the matrix to the nanoparticle in the presence interphase between the nanoparticle and the matrix. The stress concentrations were found to be low in the nanocomposites having interphase between the matrix and the nanoparticle. In the presence of voids in the interphase region the fracture was concentrated locally at the voids.

Keywords: RVE models, AlN, AA1100, finite element analysis, interphase, voids, nanocomposite.

1. Introduction

For composite materials, the aluminum nitride (AlN) nanoparticles have good interface compatibility, and can improve the mechanical properties of composite materials and the thermal conductivity of dielectric. The AlN is used for manufacturing integrated circuit board, electronic devices, optical devices, radiator, and high temperature crucible; for fabrication of metal matrix and polymer matrix composites, especially in the heat seal adhesives and electronic packaging materials and high thermally conductive ceramics.

AA1100 aluminum alloy is mechanically strongest alloy in the series of 1xxx. At the same time, it keeps the benefits of being relatively lightly alloyed (compared to other series), high electrical conductivity, corrosion resistance, and workability. This alloy is commercially pure aluminum with excellent forming characteristics. In the annealed condition the alloy can be cold worked extensively without an intermediate annealing. This alloy is commonly used in spun hollowware, fin stock, heat exchanger fins, dials and name plates, cooking utensils, decorative parts, giftware, rivets and reflectors, and in sheet metal work.

The composites are widely used in many engineering applications. The higher stiffness of ceramic particles can lead to an incremental increase in the stiffness of a composite. Of particular importance on the overall mechanical properties of a composite is the interphase which is a three dimensional region immediately surrounding the reinforced particulates. The bonding between the matrix and the reinforced particulate occurs across this region and the stiffness properties of this region differ from that of the matrix and the reinforced particulate [1, 3]. Interfacial debonding can cause shear yielding of the matrix around the particles.

The finite element procedure and analytical methods have been exceptionally effective in determining the mechanical properties of non-homogeneous materials like composites. In the finite element numerical models, very fine meshes need to be applied inside and around the interphase layers which results in large number of degrees of freedom. Currently, the use of a representative volume element (RVE) of the composite microstructure [4], in conjunction with a finite element (FE) analysis tool is well established for examining the effective material properties and understanding the micromechanics of the composite materials.

When metal matrix composites are manufactured through casting route, there is every possibility of porosity in the composites. The representative volume element (RVE) models are used considering the existence and non-existence of voids and interphase between the matrix and the inclusions. The thermo-mechanical properties of the interphase vary between those of the inclusion and those of the matrix. In the interphase region, the complex phenomena may develop around the inclusions. The phenomena may be areas of imperfect bonding, residual stresses due to shrinkage during the casting stage and the strain hardening stage, stress singularities due to rough surface of the inclusions, clustering, voids, debonding, etc. All these phenomena do not develop conditions of perfect adhesion between matrix and inclusion. The aim of this investigation is to study numerically the influence of interphase on the tensile behavior of aluminum nitride/AA1100 nanocomposites.

2. Strengthening Mechanisms

The strength of a particulate metal matrix composite depends on the strength of the weakest zone and metallurgical phenomena in it. Depending on the assumption that the stress cannot be transformed from the matrix to the reinforcement, the strength of a particulate reinforced metal matrix composite was determined from the effective sectional area of load-bearing matrix without reinforcement as given by Danusso and Tieghi [5]:

$$\sigma_c = \sigma_m(1 - v_p) \quad (1)$$

where σ_c and σ_m are, respectively, composite strength and matrix strength, and v_p is particulate volume fraction in the composite. This criterion represents that the composite strength decreases with increasing volume fraction of particulate in the composite.

Considering adhesion between filler and polymer, a lower-bound strength of the composite was derived by Nicolais and Nicodemo [6]:

$$\sigma_c = \sigma_m(1 - 1.21{v_p}^{2/3}) \quad (2)$$

An upper-bound is obtained by assuming, that the strength of the composite is simply equal to the strength of the matrix. Therefore, the strength is intermediate between these two bounds and cannot be higher than that of the matrix.

Eq. (2) was further modified considering the stress concentration of particle volume fraction by Jancar et al. [7]:

$$\sigma_c = \sigma_m(1 - 1.21{v_p}^{2/3})S_r \quad (3)$$

where S_r is a strength reduction factor and its values lie in the range from 0.2 to 1.0 for high and low volume fractions respectively. When S_r = 1.0, this criterion is equivalent to the criterion proposed by Nicolais and Nicodemo, hence the effect is same.

Eq. (2) was also further altered to include some adhesion between matrix and particulates by Lu et al. [8]:

$$\sigma_c = \sigma_m(1 - 1.07{v_p}^{2/3}) \quad (4)$$

As such modification the strength of composites is raised. Yet the issue of particle size and the obstructions of particles of dislocation are not counted. This standard is fairly more serious than the earlier criteria mentioned above.

For very strong particle-matrix interfacial bonding, an empirical relationship was proposed by Pukanszky et al. [9] as given below:

$$\sigma_c = \left[\sigma_m\left(\frac{1-v_p}{1+2.5v_p}\right)\right]e^{Bv_p} \quad (5)$$

where B is an empirical constant, which depends on the surface area of particles, particle density and interfacial bonding energy. The value of B varies between from 3.49 to 3.87.

Elastic modulus (Young's modulus) is a measure of the stiffness of a material and is a quantity used to characterize materials. Elastic modulus is the same in all orientations for the isotropic materials. Anisotropy can be seen in many composites. Based on the assumption of rigid particle, an equation was proposed by Einstein [10] to predict the modulus of elasticity of metal matrix composite as given by:

$$E_c = E_m(1 + 2.5v_p) \quad (6)$$

where E_c and E_m are Young's module of composite and matrix and v_p is the volume fraction of particles. Einstein's equation holds good only at low volume fractions of reinforcement and assumes perfect adhesion between particle and matrix, and uniform distribution of reinforced particles.

Kerner [11] found equation for estimating the modulus of a composite that contains spherical particles in a matrix as follows:

$$E_c = E_m\left(1 + \frac{v_p}{1-v_p}\frac{15(1-m_m)}{8-10m_m}\right) \quad (7)$$

For $E_p \geq E_m$ and m_m is the matrix poisson's ratio. The modulus of elasticity computed from Kerner's equation is lower than that obtained from Einstein's and Guth's equations.

The Young's modulus of particulate composites with the modified rule of mixtures is given by Fu, Xu, & Mai [12],

$$E_C = \varphi_p E_p v_p + E_m(1 - v_p) \quad (8)$$

where $0 < \varphi_p < 1$ is a particulate strengthening factor.

The Young's modulus was established by Ishai and Cohen [13] based on a uniform stress applied at the boundary as given by

$$\frac{E_c}{E_m} = 1 + \frac{1 + (\delta - 1) v_p^{2/3}}{1 + (\delta - 1)\left(v_p^{2/3} - v_p\right)} \quad (9)$$

which is upper-bound equation. Here, the particle and matrix are in a state of macroscopically homogeneous and adhesion is perfect at the interface. The lower-bound equation is given by

$$\frac{E_c}{E_m} = 1 + \frac{v_p}{\delta/(\delta - 1) - v_p^{1/3}} \quad (10)$$

where $\delta = E_p / E_m$.

3. Materials and Methods

The matrix material was AA1100 aluminum alloy. The reinforcement material was aluminum nitride (AlN) nanoparticles of average size 100nm. The mechanical properties of materials used in the present work are given in table 1.

Table 1: Mechanical properties of AA1100 matrix and AlN nanoparticles.

Property	AA1050–H16	AlN
Density, g/cc	2.705	3.26
Elastic modulus, GPa	68.90	330
Shear modulus, GPa	26	131
Bulk modulus, GPa	67.55	-
Ultimate tensile strength, MPa	145	270
Poisson's ratio	0.33	0.24

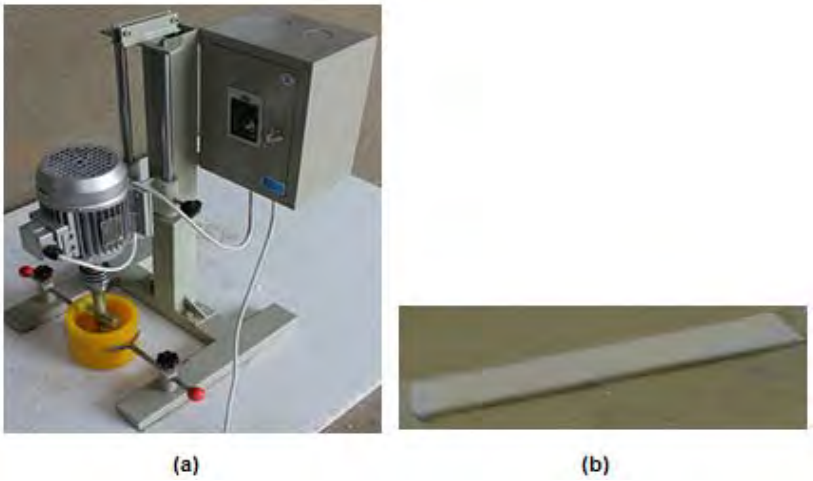

Figure 1. (a) Stir casting machine and (b) cast tensile specimen

3.1 Preparation of composite specimens

The matrix alloys and composites were prepared by the stir casting and low-pressure die casting process. The volume fractions of aluminium nitride reinforcement were 10%, 20%, and 30%. AA1100 matrix alloy was melted in a resistance furnace. The crucibles were made of graphite. The melting losses of the alloy constituents were taken into account while preparing the charge. The charge was fluxed with coverall to prevent dressing. The molten alloy was degasified by tetrachlorethane (in solid form). The crucible was taken away from the furnace and treated with sodium modifier. Then the liquid melt was allowed to cool down just below the liquidus temperature to get the melt semi solid state. At this stage, the preheated (500^0C for 1 hour)

reinforcement particles were added to the liquid melt. The molten alloy and reinforcement particles are thoroughly stirred manually for 15 minutes, as shown in figure 2. After manual steering, the semi-solid, liquid melt was reheated, to a full liquid state in the resistance furnace followed by an automatic mechanical stirring using a mixer to make the melt homogenous for about 10 minutes at 200 rpm. The temperature of melted metal was measured using a dip type thermocouple. The preheated cast iron die was filled with dross-removed melt by the compressed (3.0 bar) argon gas [14].

3.2 Strain hardening

Work hardening, also known as strain hardening or deformation hardening, is a phenomenon where the strength of a material increases during plastic deformation. The stir cast test samples were homogenized. For homogenization the test samples were heated at a constant rate of 100°C/h to 550°C, then held at 550°C for 6 hours, and slowly cooled at a rate of 6°C/h to a temperature of 350°C before quenching. The homogenized were cold rolled to get strain hardening conditions of H16 as shown in figure 2. AA1100/AlN nanocomposites were cold rolled directly from as-cast and homogenized condition in a laboratory mill at a relatively low strain rate less than 1. Lubricated rolls were used at a speed of 5m/min. The strain was calculated from the thicknesses of the test samples before and after rolling process. The strain measurements are defined by:

$$\varepsilon = \ln \frac{t_O}{t} \qquad (11)$$

where, t_o and t are thickness of the test sample before and after rolling.

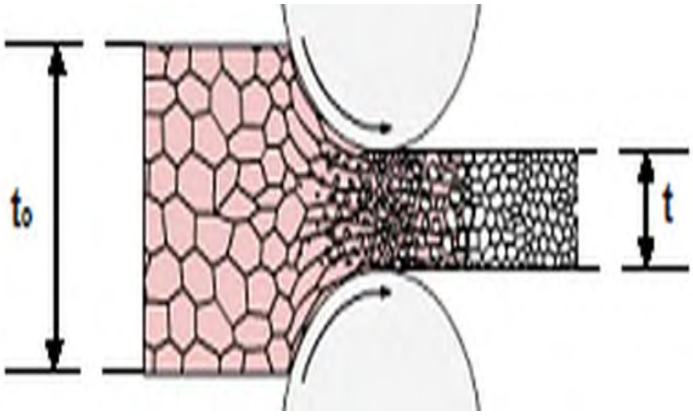

Figure 2. Strain hardening using rolling process

3.3 Tensile testing

The strain hardened samples were machined to get flat-rectangular specimens (figure 3a) for the tensile tests. The tensile specimens were placed in the grips of a Universal Test Machine (UTM) at a specified grip separation and pulled until failure. The test speed was 2 mm/min (as for ASTM D3039). A strain gauge was used to determine elongation as shown in figure 3b.

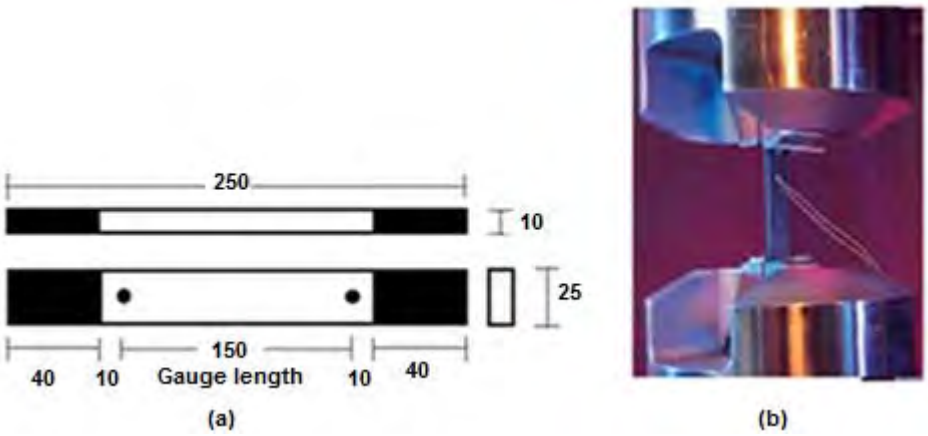

Figure 3. (a) Shape and dimensions of tensile specimen (all diemsions are in mm), and (b) Tensile testing.

3.4 Microscopic analysis

An image analyzer was used to study the distribution of the reinforcement particles within the AA6061 aluminum alloy matrix. The polished specimens were ringed with distilled water and etched with 0.5% HF solution for optical microscopic analysis. The scanning electron microscope (SEM) was used to find the interphase and to establish the microscopic mechanisms governing fracture. The scanning was carried using S-3000N Toshiba SEM.

3.5 Tensile strength, elastic and shear moduli and interphase models

The porosity problem is in fact a serious concern for nanocomposites. True density is very difficult to achieve, and some amount of residual porosity is inevitable. It is important to consider the effect of porosity when analyzing the mechanical properties of nanocomposite materials. When the nanocomposite is subjected to tensile loading, there is a possibility of debonding at the interface of matrix and reinforcement.

A new criterion was suggested by the Author [15] considering adhesion, formation of precipitates, particle size, agglomeration, voids/porosity, obstacles to the dislocation, and the interfacial reaction of the particle/matrix. The formula for the strength of composite is stated below:

$$\sigma_c = \left[\sigma_m \left\{\frac{1-(v_p+v_v)^{2/3}}{1-1.5(v_p+v_v)}\right\}\right] e^{m_p(v_p+v_v)} + kd_p^{-1/2} \qquad (12)$$

$$k = E_m m_m / E_p m_p$$

where v_v and v_p are the volume fractions of voids/porosity and particulates in the composite, m_m and m_p are the possion's ratios of the matrix and particulates, and m_m *and* m_p are Poisson's ratios of the matrix and particulate, E_m and E_p are the elastic moduli of the matrix and particulate respectively.

The equation as recommended by the Author [15] to find Young's modulus includes the effect of voids/porosity in the composite as given below:

$$\frac{E_c}{E_m} = \left(\frac{1-{v_v}^{2/3}}{1-{v_v}^{2/3}+v_v}\right) + \left(\frac{1+(\delta-1){v_p}^{2/3}}{1+(\delta-1)({v_p}^{2/3}-v_p)}\right) \qquad (13)$$

where $\delta = E_p / E_m$.

The theoretical density can be calculated by the Rule of Mixture. In the present work the percentage of voids were computed using actual and theoretical densities of the nanocomposites.

The interphase has elastic properties, which are changing with the radial distance (*r*) from the reinforcement boundary [16]. It was assumed that the variation of the elastic modulus and Poisson's ratio is linear. The elastic modulus of the interphase is given by:

$$E_i = (\alpha E_p - E_m)\left(\frac{r_i - r}{r_i - r_p}\right)^2 + E_m \qquad (14)$$

Where Ep, Em are the elastic moduli of the nanoparticle and the matrix respectively and r_i is the outer radius of the interphase; $0 \ll \alpha \ll 1$.

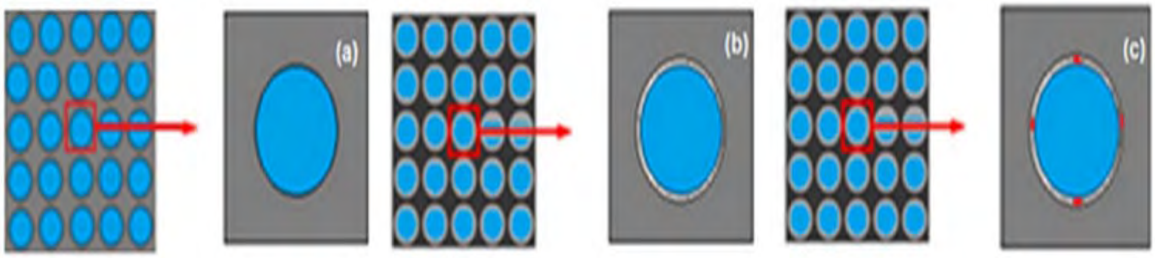

Figure 4. The RVE models.

3.5 RVE modeling using finite element analysis (FEA)

The representative volume element (RVE) is the smallest volume over which a measurement can be made that will yield a value representative of the whole. In this research, a cubical RVE was implemented to analyze the tensile behavior AA1100/AlN nanocomposites (figure 4). The determination of the RVE's dimensional conditions requires the establishment of a volumetric fraction of spherical nanoparticles in the composite. Hence, the weight fractions of the particles were converted to volume fractions. The volume fraction of a particle in the RVE is determined using equation:

$$v_p(\text{RVE}) = \frac{\text{Volume of nanoparticle}}{\text{Volume of RVE}} = \frac{16}{3} \times \left(\frac{r}{a}\right)^3 \quad (15)$$

where, r represents the particle radius and a indicates the diameter of the cylindrical RVE. The volume fraction of the particles in the composite (V_p) was chosen to be 0.10, 0.20 and 0.30 and the particle radius (r) was taken to be 100 nm.

The RVE dimension (a) was determined by equalizing equation (15). In general, the width of the grain boundary in nanocomposites materials is estimated to be about 1 nm. Three schemes of RVE models were considered. In the first scheme only adhesion was assumed between the nanoparticle and the matrix without interphase. In the second scheme an interphase was considered between the nanoparticle and the matrix. In the third scheme voids (as a result of porosity and debonding) were considered in the interphase region. The loading on the RVE was defined as symmetric displacement, which provided equal displacements at both ends of the RVE. To obtain the elastic modulus and yield strength, the force reaction was defined against displacement. The large strain PLANE183 element was used in the matrix and the interphase regions in all the models (table 2). In order to model the adhesion between the interphase and the particle, a COMBIN14 spring-damper element was used. The stiffness of this element was taken as unity for perfect bonding which can determine the interfacial strength for the interface region.

Table 2: Elements features, applications and size ranges used in RVE modeling.

Element code	Plane 183	Contact 172	Combination 14	Target 169
Feature	Quadrilateral-8 nodes	Linear 3 node	Longitudinal spring-damper	Shape complexity
Application	Matrix and interphase	Interface contact	Elastic modeling of adhesion	Contact bodies

To converge an exact nonlinear solution, it is also important to set the strain rates of the FEM models based on the experimental tensile tests' setups. Hence, FEM models of different RVEs with various particle contents should have comparable error values. In this respect, the ratio of the tensile test speed to the gauge length of the specimens should be equal to the corresponding ratio in the RVE displacement model. Therefore, the rate of displacement in the RVEs was set to be 2.0 (1/min).

The two-dimensional RVE model was modeled using the plain strain conditions which were defined as a deformation state in which w = 0 everywhere and u and v were functions of x and y, but not of z thus, $\varepsilon_{yz} = \varepsilon_{zx} = 0$. Then for isotropic and isothermal conditions [17] the stress-strain relation is given by

$$\begin{Bmatrix} \sigma_x \\ \sigma_y \\ \sigma_{xy} \end{Bmatrix} = \frac{E}{(1+m)(1-2m)} \begin{bmatrix} 1-m & m & 0 \\ m & 1-m & 0 \\ 0 & 0 & \frac{1-2m}{2} \end{bmatrix} \begin{Bmatrix} \varepsilon_x \\ \varepsilon_y \\ \varepsilon_y \end{Bmatrix} \quad (16)$$

The shear modulus is given by

$$G = \frac{E}{2(1+m)} \quad (17)$$

$$\varepsilon_x = \frac{\sigma_x}{E} - m\frac{\sigma_y}{E} \quad (18)$$

$$\varepsilon_y = \frac{\sigma_y}{E} - m\frac{\sigma_x}{E} \quad (19)$$

$$\varepsilon_{xy} = \frac{\sigma_{xy}}{G} \quad (20)$$

where, σ_x and σ_y are the stresses along x- and y-directions of the composite, σ_{xy} is the shear stress in the xy-plane, m is the Poisson's ratio, ε_x and ε_y are the strains along x- and y-directions of the composite, ε_{xy} is the shear strain in the xy-plane, and E and G are the elastic and shear moduli of the composite respectively.

4. Results and Discussion

Figure 5 reveals that the AlN nanoparticles are randomly distributed in the AA1100 matrix. Table 3 depicts the tensile strengths of the nanocomposites obtained by FEA (RVE models), empirical models proposed by Danusso and Tieghi, Nicolais and Nicodemo, Lu et al, Pukanszky et al, the author, and obtained by the experimental procedure. Danusso and Tieghi [5], Nicolais and Nicodemo [6] and Lu et al criteria [8] criteria represent that the composite strength decreases with increasing volume fraction of particulate in the composite. Danusso and Tieghi [5], and Nicolais and Nicodemo [6] did not include the strengthening mechanism due to the formation of precipitates at the particulate/matrix interface and deformation by the particulates. Lu et al criterion [8] also did not consider the issue of particle size and the behavior of particles in the composite. All these three criteria yield

the composite strength always lower than that of the matrix. Pukanszky et al criterion [9] has taken care of the presence of particulates in the composite and interfacial bonding between the particle/matrix. The effect of particle size and voids/porosity are not considered in this criterion. This criterion characterizes that the composite strength increases with increasing volume fraction of particulate in the composite.

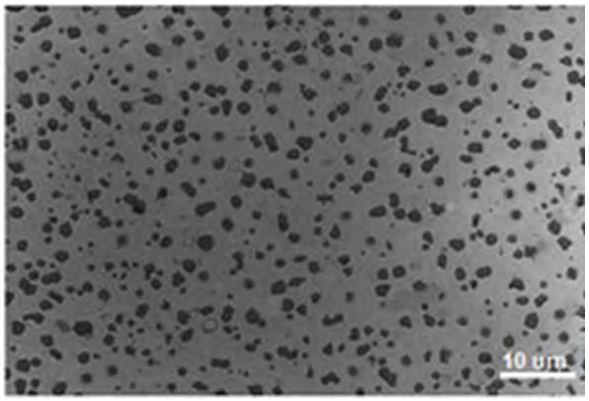

Fig.5. Microstructure of strain hardened AA1100/AlN nanocomposite (305 Vp).

The Author's model includes the effect of interphase, nanoparticle behavior and voids present in the nanocomposite. In the presence of voids in the nanocomposite, the interface region between the nanoparticle and the matrix gets stiffened and consequently this leads the slow rate of increasing (or remain constant) the tensile strength with an increase in the nanoparticles content. The tensile strengths obtained from the RVE model with interphase and voids are in good agreement with the experimental results and Author's model as given in table 3. The nonlinear deformation behavior of the reinforcements and the matrix/reinforcement debonding are considered in the RVE models. These micromechanical factors are important in the large plastic deformation regime.

Table 3: Tensile strength obtained from different criteria.

Criteria	Tensile strength, MPa		
	10% Vp	20% Vp	30% Vp
Danusso and Tieghi	130.500	116.000	101.500
Nicolais and Nicodemo	107.200	84.997	66.374
Lu et al	111.570	91.940	75.470
Pukanszky et al	150.842	161.439	174.940
Author-without voids	142.260	148.170	161.520
Author-with interphase and voids	142.670	150.610	167.330
RVE-without interphase	135.103	143.263	153.186
RVE-with interphase	142.233	150.448	167.221
RVE-with interphase and voids	143.378	153.855	169.877
Experimental	143.200	152.120	168.900

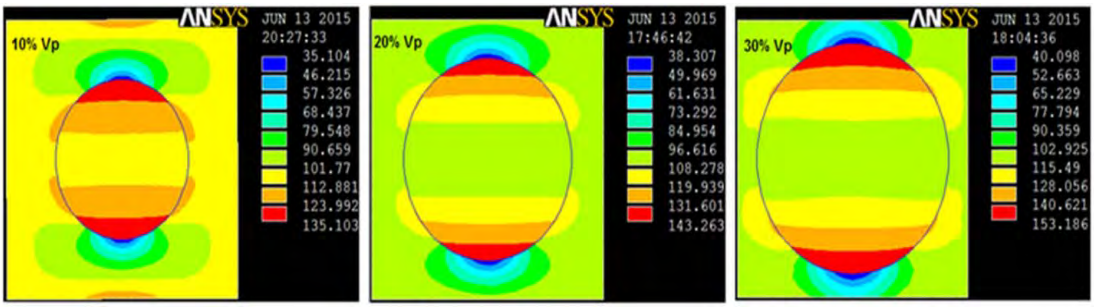

Figure 6. Tensile strength along load direction without interphase.

Barely consideration of adhesive bonding between the matrix and aluminum nitride nanoparticle, the debonding is occurred at the particle/matrix interface region in the nanocomposite, as shown in figure 6. The debonding

between the matrix and the nanoparticle is owing to shearing of the matrix material adhered to the nanoparticle. The aluminum nitride nanoparticle is not ruptured. This is because of the stress induced in the aluminum nitride nanoparticle is below its tensile strength of 270 MPa. The transport of load from the matrix to the nanoparticle is merely small as in support of the stress contours appeared in the matrix and the nanoparticle. This is not the practical situation of the composites. Hence, there must be a chemical reaction between the matrix and the nanoparticle forming an interphase to bond them as shown in Fig.7. With the existence of the interphase region, some researchers have gone on to consider this region as being a homogeneous region with constant properties [18].

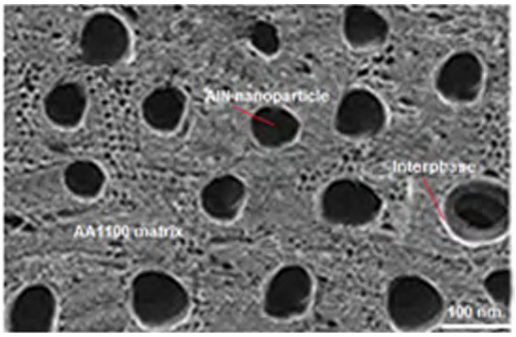

Figure 7. Interphase around AlN nanoparticle.

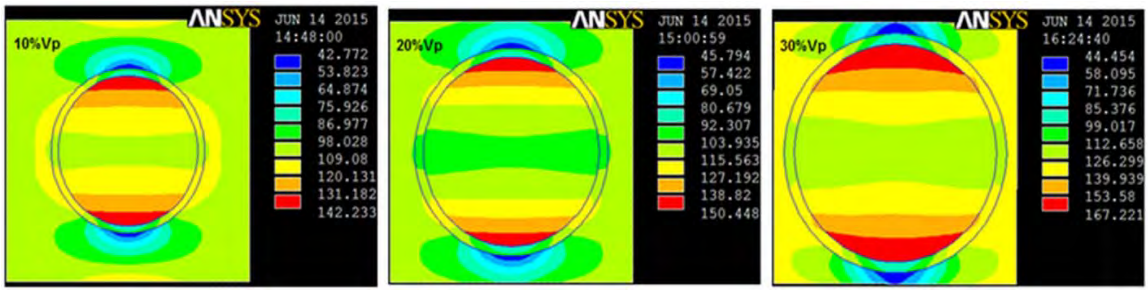

Figure 8. Tensile strength along load direction with interphase.

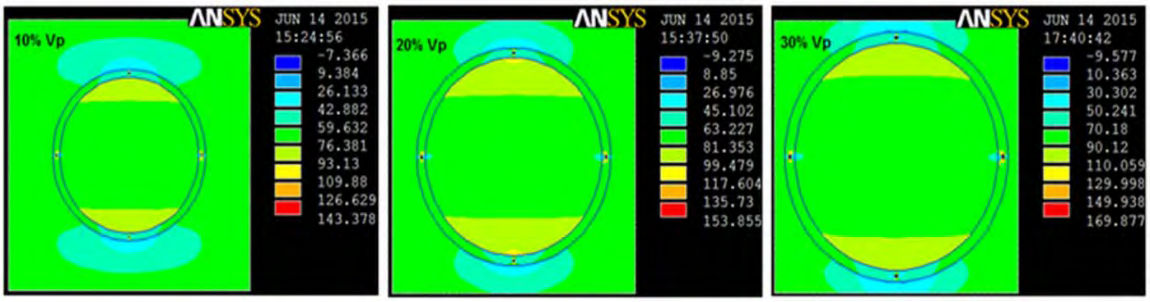

Figure 9. Tensile strength along load direction with interphase and voids.

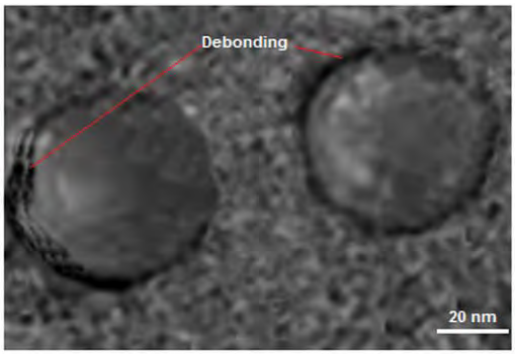

Figure 10. Debonding at the interface of nanoparticle (30% Vp) and matrix.

Figure 8 shows the effect of interphase between the nanoparticle and the matrix on the stress induced in the nanocomposite in the direction of tensile loading. Here also, the tensile strength increases with increasing content of AlN nanoparticle in the AA1100 matrix. The transport of load from the matrix to the nanoparticle is

considerably improved as understood from the stress contours appeared in the matrix and the nanoparticle. Figure 9 shows the effect of voids in the interphase region on the stress induced in the nanocomposite. In the present work, the voids are considered in the longitudinal and the transverse direction of the tensile loading. In the presence of voids there are stress concentrations around them. In the composite, there is an evidence of breakage of bonding not only between the nanoparticle and the interphase but also between the matrix and the interphase (figure 10).

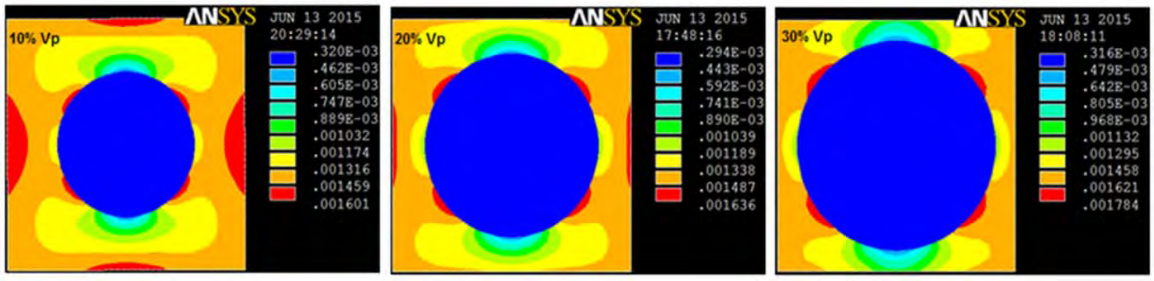

Figure 11. Tensile strain along load direction without interphase.

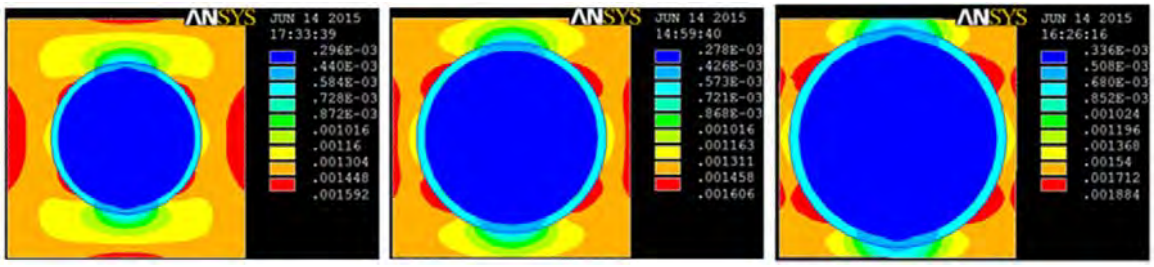

Figure 12. Tensile strain along load direction with interphase.

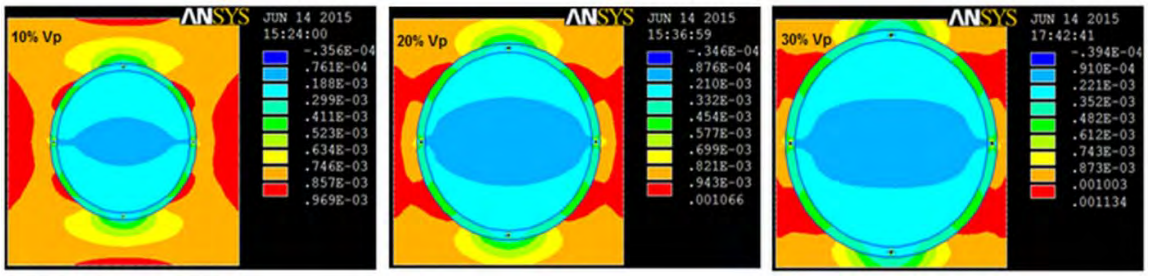

Figure 13. Tensile strain along load direction with voids and interphase.

Figures 11, 12 and 13 show the tensile strain contours of the RVE models for the situation involving without interphase, with interphase and with voids and interphase respectively. According to Figures 11, 12 and 13, the RVE is expanded elastically away from the particle in the direction of the tensile loading. This increases the contact area between the particle and the matrix in the perpendicular direction to the tensile loading and decreases the contact area between the particle and the matrix in the direction of the tensile loading. In addition, the deformation is propagated in the normal direction to the tensile loading. It is also observed that the strain induced is higher in the nanocomposites without interphase and voids than that induced in the nanocomposites with interphase or voids and interphase. This is on account of an increase in the stiffness of the nanocomposite.

Table 4 gives the elastic moduli of the nanocomposites obtained by Einstein criterion [10], Kerner criterion [11], Rule of Mixture [12], Ishai and Cohen [13], the RVE models and the Author's models. Einstein criteria [10] holds good only at low volume fractions of reinforcement and assumes perfect adhesion between particle and matrix, and uniform distribution of reinforced particles. The Young's modulus computed using Einstein's equation is independent of particle size and increases linearly with increasing of particle loading in the composite. The modulus of elasticity computed from Kerner criteria [11] is lower than that obtained from Einstein criteria. Ishai and Cohen [13] have assumed that the particle and matrix are in a state of macroscopically homogeneous and adhesion is perfect at the interface. For the nanocomposites without voids the elastic modulus obtained by the Author's model is nearly equal to Einstein criteria. For the nanocomposites with voids and the interphase the elastic modulus obtained by the Author's model is nearly equal to Ishai and Cohen criteria [13]. The elastic modulus decreases in the presence of voids in the nanocomposites. This is clearly observed with nanocomposites having 30% AlN. Sanders et al. [19] attributed the observed decrease of Young's modulus to a slight porosity in the samples.

Table 4: Elastic modulus obtained from different models.

Criteria	Elastic modulus, GPa		
	10% Vp	20% Vp	30% Vp
Einstein	86.13	103.35	120.58
Kerner	80.38	94.72	113.17
Rule of Mixture	78.51	88.12	97.73
Ishai and Cohen	155.96	171.75	187.97
Author's model-without interphase	87.06	102.85	119.07
Author's model -with voids and interphase	155.96	169.99	185.83
RVE-without interphase	84.39	87.57	85.87
RVE-with interphase	89.34	93.68	88.76
RVE-with voids and interphase	147.97	144.14	149.80

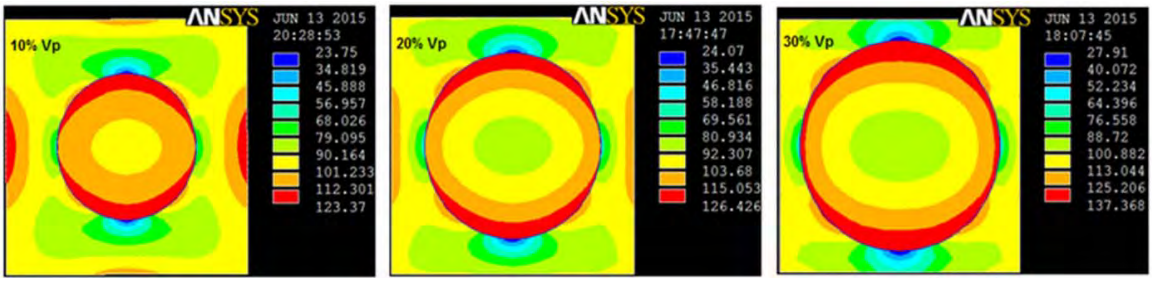

Figure 14. von Mises stress without interphase.

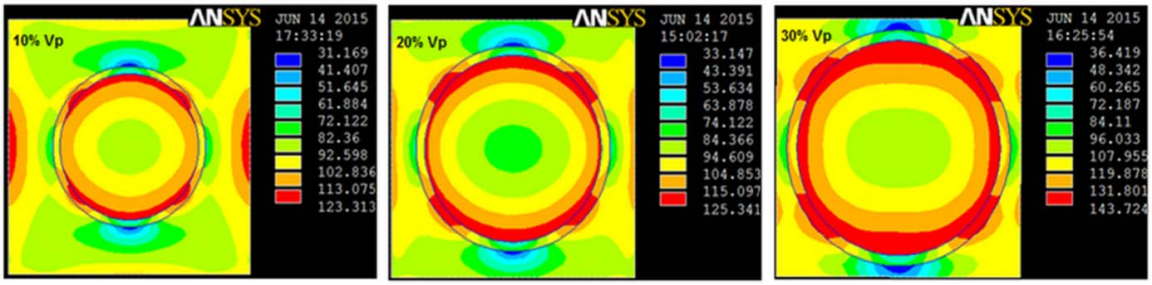

Fig.15. von Mises stress with interphase.

Figure 14 shows the variation of von Mises stress in the nanocomposite without interphase. The adhesion strength at the interface determines the load transfer between the components. Effective stress transfer is the most important factor which contributes to the strength of two-phase composite materials. Discontinuity in the form of debonding exists because of non-adherence of particle to matrix. However, for strain hardened nanocomposites, enhancement of matrix adhesion to the nanoparticle will lead to an increase in strength especially for nanoparticles with high surface areas. It is observed from Fig.14 that the debonding occurs at the entire periphery of the nano particle without interphase between the nanoparticle and the matrix. Hence, the stress transfer from the matrix to the nanoparticle becomes less for the nanocomposites without interphase. It is noticed from figure 15 that the debonding occurs at the partial periphery of the interphase between the nanoparticle and the matrix. Hence, the stress transfer from the matrix to the nanoparticle becomes high for the nanocomposites with interphase. It is also observed from figure 16 that the fracture is confined to the regions where the voids are present in the interphase.

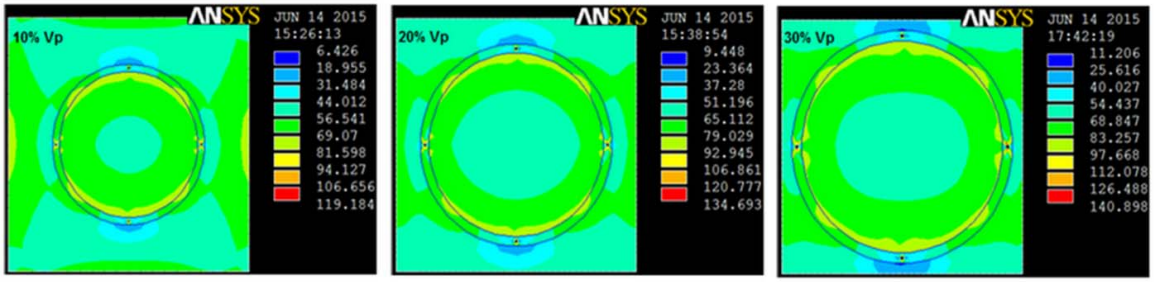

Fig.16. von Mises stress with voids and interphase.

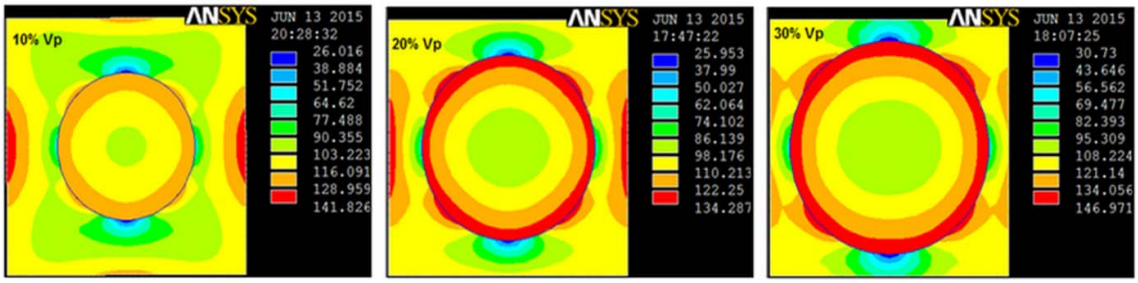

Fig.17. Stress intensity without interphase.

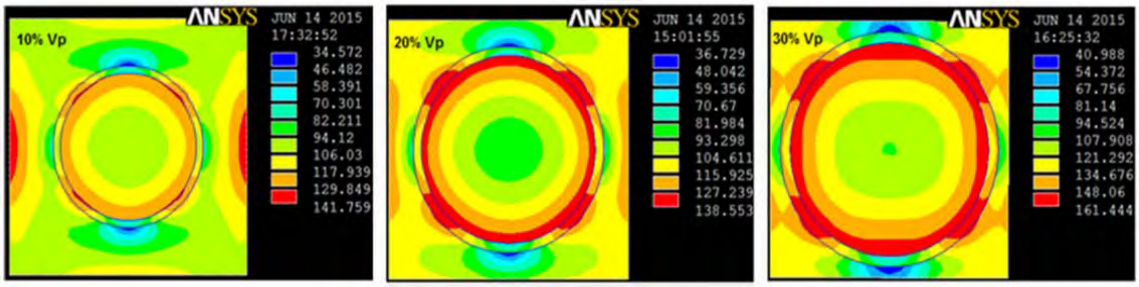

Fig.18. Stress intensity with interphase.

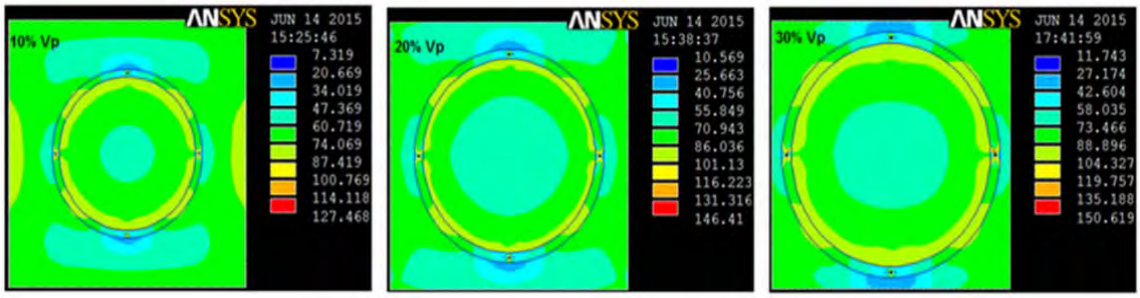

Fig.19. Stress intensity with voids and interphase.

The stress concentrations around the nanoparticle can be visualized from figures 17, 18 and 19 in the nanocomposites without interphase, with interphase and with voids and interphase respectively. The stress concentration is higher in the nanocomposites without interphase between the matrix and the nanoparticle than in the nanocomposites with interphase between the matrix and nanoparticle and with voids in the interphase region. It is observed that the interfacial debonding is high between the particle and the matrix because of high local stress concentration around the nanoparticle in the nanocomposites without interphase. The plastic flows are initiated within the matrix and ended at the nanoparticle/matrix interface. Owing to high tensile strength of the nanoparticles, the plastic deformation becomes concentrated at several locations in the matrix. The localized strain is also observed around the particle because of the high load-transfer effect in particles. The plastic behavior is differed considerably with inclusion of interphase between the nanoparticle and the matrix. As the pressure is increased on the RVE model, the plastic strain zone is expanded resulting in a plastic deformation of the interphase between the nanoparticle and the matrix. In the present work the interphase and the nano particle are stiffer than the matrix. The elastic moduli (stiffness) of AlN nanoparticle, interphase, AA1100 matrix are 330 GPa, 165 GPa (without voids), and 69 GPa respectively.

5. Conclusion

Without interphase and barely consideration of adhesive bonding, the debonding is occurred at the particle/matrix interface region in the nanocomposite. The stress concentrations are high in the nanocomposites without interphase between the nanoparticle and the matrix. Due to interphase between the nanoparticle and the matrix, the nanoparticles are not overloaded during the transfer of load from the matrix to the nanoparticle via the interphase. The tensile strengths obtained by the Author's model (with voids) and experimental results have been found nearly equal. In the case of nanocomposites with voids in the interphase region, the debonding is concentrated at voids but not at the entire periphery of the interphase between the matrix and the nanoparticle. For strain hardened nanocomposites, there is an enhancement of adhesion between the nanoparticle and the matrix.

References

[1] B. Kotiveerachari and A. Chennakesava Reddy, Interfacial effect on the fracture mechanism in GFRP composites, CEMILAC Conference, Ministry of Defence, India, B85-87, 1999.

[2] A. Chennakesava Reddy, Analysis of the relationship between the interface structure and the strength of carbon-aluminum composites, NATCON-ME, Bangalore, pp.61-6, 2004.

[3] A. Chennakesava Reddy, Mechanical properties and fracture behavior of 6061/SiCp Metal Matrix Composites Fabricated by Low Pressure Die Casting Process, Journal of Manufacturing Technology Research, vol.01, no.3/4, pp.273-286, 2009.

[4] R. Hill, Elastic properties of reinforced solids: some theoretical principles, Journal of the Mechanics and Physics of Solids, 11, 357-372, 1963.

[5] F. Danusso and G. Tieghi, Strength versus composition of rigid matrix particulate composites, Polymer, vol.27, pp.1385-1390, 1986.

[6] L. Nicolasis and L.Nicodemo, Strength of particulate composite, Polymer Engineering and Science, vol.13, pp.469-475, 1973.

[7] J. Jancar, A. Dianselmo and A.T. Dibenedetto, The yield strength of particulate reinforced thermoplastic composites, Polymer Engineering and Science, vol.32, pp.1394-1399, 1992.

[8] S. Lu, L. Yan, X. Zhu and Z.Qi, Microdamage and interfacial adhesion in glass bead-filled high-density polyethylene, Journal of Materials Science, vol.27, pp.4633-4638, 1992.

[9] B. Punkanszky, B. Turcsanyi and F.Tudos, Effect of interfacial interaction on the tensile yield stress of polymer composites, In: H. Ishida, editor, Interfaces in polymer, ceramic and metal matrix composites, Amsterdam: Elsevier, pp.467-477, 1988.

[10] A. Einstein, Investigation on theory of Brownian motion. New York: Dover, 1956.

[11] E.H.Kerner, The elastic and thermoelastic properties of composite media, Proceedings of the Physical Society B, vol.69, pp.808-813, 1956.

[12] S.Y. Fu, G. Xu and T.W. Mai, On the elastic modulus of hybrid, particle/short fiber/polymer composites, Composite Part B, vol.33, pp.291-299, 2002.

[13] O. Ishai and I.J.Cohen, Elastic properties of filled and porous epoxy composites, International Journal of Mechanical Sciences, vol.9, pp.539-546, 1967.

[14] A. Chennakesava Reddy, Tensile fracture behavior of 7072/SiCp metal matrix composites fabricated by gravity die casting process. Materials Technology: Advanced Performance Materials, vol.26, pp.257-262, 2011.

[15] A. Chennakesava Reddy, Influence of particle size, precipitates, particle cracking, porosity and clustering of particles on tensile strength of 6061/SiCp metal matrix composites and validation using FEA, International Journal of Material Sciences and Manufacturing Engineering, vol.42, pp.1176-1186, 2015.

[16] D.F. Adams and S.W. Tsai, The influence of random filament packing on the transverse stiffness of unidirectional composites, Journal of Composite Materials, vol.3, pp.368, 1969.

[17] Chennakesava R Alavala, Finite element methods: basic concepts and applications, PHI Learning Private Limited, New Delhi, 2007.

[18] K.W. Yu, G.Q. Gu and J.P. Huang, Dielectric response of spherical particles of graded materials, Conducting-Materials, e-print arXiv:0211532, 2002.

[19] P.G. Sanders, J.A. Eastman and J.R.Weertman, Elastic and tensile behavior of nanocrystalline copper and palladium, Acta Materialia, Vol.45, pp.4019-4025, 1997.